GIBBSITE TO BOEHMITE TRANSFORMATION IN STRONGLY CAUSTIC AND NITRATE ENVIRONMENTS

X. Gong,[1] Z. Nie,[1] M. Qian,[1] J. Liu,[1]

L. A. Pederson,[1] D. T. Hobbs,[2]* and N. G. McDuffie[3]

[1]Pacific Northwest National Laboratory, Richland, WA 99352

[2]Westinghouse Savannah River Company, Aiken, SC 29808

[3]1745 S.W. Whiteside Drive, Corvallis, OR 97333

*Corresponding author: Westinghouse Savannah River Company
Aiken, SC 29808

ABSTRACT

The transformation of gibbsite to boehmite in strongly caustic solutions was studied using quantitative X-ray diffraction, Fourier transform infrared spectroscopy, and transmission electron microscopy techniques. Under hydrothermal conditions we identified two transformation mechanisms; (1) dehydration and in-situ nucleation and (2) dissolution and nucleation. If the reaction container was not completely sealed, dehydration of gibbsite followed by in-situ nucleation of boehmite was the preferred mechanism. Boehmite produced fibrous boehmite particles within the amorphous matrix of the decomposed gibbsite particles, which exhibited a poorly crystalline structure and smaller size than the initial gibbsite particles. In a closed environment, the preferred mechanism was the dissolution of gibbsite along (001) planes. The final boehmite particles were not morphologically related to the initial gibbsite particles and could be many times larger than the gibbsite particles.

Key Words: Gibbsite, boehmite, transformation, dehydration, precipitation, dissolution, aluminate

INTRODUCTION

Gibbsite (α-aluminum trihydroxide, α-$Al(OH)_3$), and boehmite (α-aluminum oxyhydroxide, α-AlOOH), are the most common aluminum hydroxide and oxyhydroxide minerals in nature.[1] The relative stability and the transformation of gibbsite and boehmite play important roles in many industrial processes, such as in the preparation of high purity alumina ceramics, absorbents and high surface area catalyst supports.[1,2] The dehydration process from gibbsite to boehmite, to γ-alumina, and finally to α-alumina is widely encountered. In the literature, the hydrothermal stability regions for alumina-water system have been well established.[1] When heated, as in a calcination process or under pressure in the presence of water, gibbsite is converted to boehmite.[3,4]

The relative stability of gibbsite and boehmite phases is also of importance to the disposal of the large quantity of high-level nuclear waste (HLW) stored at the U.S. Department of Energy sites. Approximately 400 millions liters of HLW are stored in underground tanks at the Hanford and Savannah River sites.[5-7] These tank wastes consist of solids (primarily metal hydroxides and hydrated metal oxides commonly referred to as sludge) and strongly alkaline high ionic strength salt solutions. The majority of the tank wastes feature non-radioactive elements including aluminum as one of the principle components.

Processes developed or under development for the permanent disposal of the HLW feature separation of the radionuclides from the bulk of the waste and immobilizing this fraction into a durable borosilicate glass wasteform.[7] In this disposal scheme the bulk of the sludge solids would process into the borosilicate glass. The total quantity of vitrified HLW is

influenced by the quantity of aluminum in the waste sludges. Aluminum also plays a direct role in the vitrification chemistry. At moderate levels aluminum assists in glass forming. However, at elevated levels aluminum can increase the viscosity of the molten glass, which adversely impacts the glass production rate and the volume of glass produced.

Current plans include a caustic leaching step to reduce aluminum levels in the sludge solids. The efficiency of the caustic leaching step varies depending on the aluminum-containing phases present in the sludge. Gibbsite readily dissolves at moderate hydroxide concentrations and temperatures. Boehmite dissolution, however, requires more rigorous conditions and generally is kinetically slow. As a result, caustic leaching of sludges high in boehmite may not be cost effective or possible in existing or planned facilities.

Conditions under which the HLW sludges have been stored include a wide range of ionic strengths, temperatures and water content. Typically the alkaline salt solutions in contact with the sludge solids contain 1.0 molar or higher sodium hydroxide. Other major components include sodium salts of nitrate, nitrite, carbonate and aluminate. Fresh HLW slurries frequently self heat due to radioactive decay to between 100 and 150 °C, with isolated regions within the storage tanks recorded as high as 350 °C for relatively short periods of time. In some tanks the supernatant liquid has been drained or allowed to evaporate to dryness. As a result of these storage conditions, a large fraction of the gibbsite may have transformed into boehmite. We initiated this testing to begin a systematic study of the tranformation of gibbsite into boehmite under conditions pertinent to the storage and pretreatment of HLW sludges to provide a more complete understanding of the aluminum-

containing mineral phases that would be present in HLW sludges after long periods of storage in underground tanks.

EXPERIMENTAL

Gibbsite was purchased from Alcoa Chemicals. Particle size ranges from 0.2 μm to 1 μm in diameter and the particles are roughly rectangular in shape. Sodium hydroxide (NaOH), ferric nitrate ($Fe(NO_3)_3 \cdot 9H_2O$), potassium permanganate ($KMn0_4$), and manganese nitrate ($Mn(NO_3)_3$) were purchased as reagent grade chemicals from Aldrich. The aqueous solutions were prepared containing 33% of the appropriate salt by weight. The salt content contained either 100% gibbsite or 70% gibbsite plus 30% of ferric nitrate, potassium permanganate, and manganese nitrate by weight (Table 1). Sodium hydroxide was added to obtain to produce a hydroxide concentration of 1.5 molal or 3.0 molal. The solutions were kept in either well-sealed or closed, but not sealed, Teflon containers at selected temperatures for varying periods of time. At the conclusion of the holding time, the solid products were separated from the supernatant liquid by filtration, washed with several portions of deionized water and the solids dried for 16 – 64 hours at ambient laboratory temperature..

Initial characterization of the solids featured a X-ray diffraction (XRD) technique using a Philips X'Pert MPD X-ray Powder Diffractometer with Cu anode (Model PW3040/00) operating at 40 kV and 50 mA and scanning rate of 0.04°/sec from 2θ 10° through 70°. Data were processed using the X'Pert Organizer software. Based on their peak areas, the relative content of each mineral phase, such as gibbsite, boehmite, or bayerite was estimated.[21]

The solids were also characterized by Infrared Spectroscopy (IR) using a Nicolet MAGNA-IR 860 spectrometer with attenuated total reflectance (ATR) and a MCT-A detector. The ATR accessory used was a Spectra-Tech ARK with a ZnSe crystal. Transmission electron microscopy (TEM) characterization consisted of dispersing fine powder sub-samples in deionized water and depositing onto 300-mesh copper TEM grids with carbon film. TEM analyses featuried a JEOL 1200 TEM at 120 kV using a single tilt stage. Select area diffraction (SAD) patterns, bright field (BF) images, dark field (DF) images and electron dispersive x-ray (EDS) spectra were obtained for all samples.

RESULTS

Transformation at Low Water Vapor Pressure

In one set of experiments, heating of the gibbsite was carried out in 1.5 molal NaOH solution at 150°C with the reaction vessel closed, but not completely sealed. This allowed water to evaporate from the cautic solution. After four hours of heating, we observed no free water in the test vessel. The rate or extent of water loss was not measured in these experiments.

Figure 1shows the XRD patterns of the isolated solids after heating for different lengths of times. We observed very broad peaks corresponding to boehmite after heating for 2.5 hours. The XRD pattern of gibbsite in Figure 1b became significantly broadened as compared with Figure 1a, indicating that the gibbsite had lost crystallinity during the first hour of heating. This trend continued in Figure 1c (2 hrs), which showed even more broadened

peaks and reduced intensity. At 2.5 hours (Figure 1d), the signature peaks of gibbsite had almost completely disappeared and broad peaks characteristic of boehmite appeared. The boehmite peaks continued to sharpen as function of time after 2.5 hours. Note that in this series, the final product contained only boehmite. No bayerite formed in the unsealed container.

Figure 2 presents the relative amount of gibbsite and boehmite estimated from the XRD peak areas. All gibbsite disappeared after 3.5 hours of heating at 150°C. The transformation to boehmite occurred relatively fast in the unsealed container. We attribute the fast conversion to the decreased water vapor pressure resulting from the open container. This observation extends similar findings reported by Candela and Perlmutter[8,9] at near neutral pH conditions to a strongly alkaline environment.

Note that the true decomposition rate of gibbsite was even faster than that shown in Figure 2, since the amorphous product of the decomposition of gibbsite is not quantified by the XRD method. The formation of an amorphous phase preceded the formation of the boehmite phase, which is not reflected in data used to generate the graph in Figure 2. For example, Figure 1 clearly reveals that at 2 hours (Figure 1c), the amount of gibbsite crystalline phase was significantly reduced, even though no significant amount of boehmite was detected yet indicating the transformation of the crystalline gibbsite phase into a phase that is amorphous by XRD analysis.

Figure 3 presents FTIR spectra recorded up to total heating time of 3.5 hours. The gibbsite peaks at 1040 and 970 cm^{-1} broaden and weaken with time. A weak, broad peak for boehmite at 1065 cm^{-1} appears at 3 hours. The intensity and sharpness of the 1065 cm^{-1} peak does not change appreciably with heating times from between 3.5 hours and 24 hours. FTIR spectral characteristics for the boehmite formed in this test series suggest a poorly or disordered crystalline structure of the boehmite formed under these conditions. The FTIR results are in agreement with the XRD data (Figure 1), which show broad diffraction peaks for boehmite.

Figure 4a shows a TEM micrograph of one particle (center particle marked B) after being heated for 2.5 hrs in the unsealed container. Some shrinkage cracks were observed along the (001) planes, due to dehydration and delamination along (001) planes. Similar changes in the morphology of of gibbsite particles has been reported in the literature during calcination.[7]

The particle shown in Figure 4a was initially a gibbsite particle and has retained the original shape. However, selected area diffraction (Figure 4b) suggests that this particle is now made up mostly of boehmite crystallites. The continuous thin rings also suggest the boehmite particles were extremely small, which explains why they are not visible in the bright field image in Figure 4a. In the low left comer of Figure 4a (marked A), a gibbsite particle is shown. The difference between gibbsite and boehmite can also be verified through EDS spectra (Figure 4c). Gibbsite has a different oxygen:aluminum ratio (O/Al = 3) than boehmite

(O/Al = 2), which is apparent in EDS spectra recorded for regions marked A and B of Figure 4a.

We also used selected area diffraction and dark field techniques to ascertain additional characteristics concerning the tranformation of gibbsite at lower water vapor pressures. Figure 5a is the bright field image of a partially converted gibbsite particle at 2.5 hours, with the selected area diffraction pattern shown in the insert. The dark field image of Figure 5b was obtained using spot pattern of (1 0 4) beam of gibbsite. This dark field image shows that this gibbsite particle was already partially decomposed, leaving behind flake-like residuals. Figure 5c shows the dark field image obtained using ring pattern of (0 6 0) beam of boehmite, clearly revealing where the boehmite particles were formed. Figure 5c shows that tiny boehmite crystallites, about 2 nm in size, were clustered in a linear fashion, either along the particle surface, or within the internal surfaces created by the decomposition of gibbsite. Figure 5d shows the dark field image obtained using ring pattern of (0 2 2) beam of boehmite. Again, clusters of small boehmite crystallites were observed on the surface of, and within the large particle.

After 4.5 hours, most of the boehmite particles were formed, as shown in Figure 6, together with the diffraction pattern. These particles were fibrous in morphology, about 100 nm in length, and a few nanometers in width. The contour of the original gibbsite particle is still obvious in Figure 6 with the boehmite particles embedded within the amorphous matrix of the original gibbsite particle.

Transformation at High Water Vapor Pressure

Figure 7 presents the XRD patterns of the reaction products obtained by heating gibbsite in a l.5 molal NaOH solution at 150°C in a sealed container for 0 – 24 hours. In this set of experiments no evaporative loss of water occurs. Initially only sharp XRD peaks from gibbsite were observed. After 2 hours (Figure 7c), a small peak at 2θ 14.4° appeared, indicating the onset of boehmite formation. This boehmite peak grew rapidly from 2 hours to 4.5 hours, at the same time the intensity of the peak at 2θ 18.2° from the gibbsite phase decreased dramatically and became zero at 4.5 hours. At 2 hours (the onset of boehmite formation), another small peak appeared at 2θ 18.7°. This peak can be attributed to another aluminum hydroxide phase, bayerite (β aluminum trihydroxide).

Figure 8 provides a plot of the weight percentage of gibbsite, boehmite, and bayerite phases versus heating time. Little tranformation of the gibbsite occurred before 2 hours. After 2 hours, the reaction rapidly accelerated. Most of the reactions complete within 5 hours. The bulk of the gibbsite transforms into boehmite. The final composition contained 85 wt % boehmite and 15 wt % bayerite. Comparison of Figures 2 and 8 reveal that the onset and rate of conversion of gibbsite to boehmite occurs faster in the unsealed container (i.e., lower water vapor pressure) experiments. This result is consistent with reports in the literature, which indicate that the conversion rate is inversely proportional to the square of the water vapor pressure.[8,9]

The results obtained from FTIR (see Figure 9) are consistent with those from XRD. FTIR spectra (a), (b) and (c) in Figure 9 are typical of gibbsite, with one peak at 1040 cm^{-1},

and one at 970 cm^{-1}. An additional peak appeared at 1065 cm^{-1} after 2.5 hours (Figure 9d), indicating the formation of boehmite. The gibbsite peak at 1040 cm^{-1} disappeared after 4.5 hours (Figure 9e), while the boehmite peak at 1065 cm^{-1} continued to grow. No other peaks were observed in the FTIR spectra. Since FTIR is sensitive to the chemical environment of the aluminum atoms, the absence of additional peaks suggests that there was no amorphous or transitional phase formed during the conversion of gibbsite into boehmite.

Note that the boehmite peak at 1065 cm^{-1} in FTIR spectra (Figure 9) continued to increase and became sharper after 4.5 hours with little or no change in relative fraction of boehmite from the XRD measurements. We attribute the FTIR spectral changes either to the ripening of the boehmite particles, which eliminates crystal defects or to the continued growth of boehmite particles from aluminum dissolved in the 1.5 molal sodium hydroxide solution. The solubility of aluminum in 1.5 molal NaOH solution is approximately 0.08 molal,[22] which is sufficiently high to account for the quantity of gibbsite present in the test.

TEM provided direct evidence that the gibbsite to boehmite transformation was through a dissolution and nucleation mechanism. Figure 10a shows the initial rectangular gibbsite particles. The particle diameter ranges from 0.2 μm to 1 μm. After heating for 2.5 hours, dissolution occurred along the (001) planes in gibbsite particles (Figure 10b), creating parallel gaps in the particles. In some of the areas, the particles were so corroded by the dissolution process that delamination of the particles was observed, leaving a brush like surface on the gibbsite particles (Figure 10c). In all cases, we did not find any evidence that the boehmite particles were directly associated with the gibbsite particles (e.g., deposited in

the gibbsite or growing from the gibbsite surface) throughout the time that gibbsite mass loss occurred. After 6.5 hours, we no longer observed any gibbsite particles, but did see evidence of bayerite particles in addition to boehmite particles (see Figure 10e). The bayerite region had a higher oxygen content than the boehmite region as evidenced by EDS spectra in Figure 10f. Currently we do not have sufficient data to determine if bayerite formed directly from gibbsite, or formed by nucleation from the solution.

Effects of Other Metals and Sodium Hydroxide Concentration

Figure 11 presents a graph of the weight percent of gibbsite and boehmite as a function of time upon heating gibbsite at 150 °C with or without the presence of iron and a mixture of iron and manganese in an unsealed vessel. In these tests we added the iron as a ferric nitrate salt, $Fe(NO_3)_3$ and the manganese as both potassium permanganate, $KMnO_4$, and manganese(II) nitrate, $Mn(NO_3)_2$ to the NaOH solution. The ferric and manganous salts precipitated immediately as metal hydroxides or hydrous metal oxides. The permanganate initially is soluble, but slowly decomposes to produce manganese oxide solids. Note that the free hydroxide concentration in solution in these tests is considerably less than that in the tests without the added metal salts. The added metal salts react with hydroxide to precipitate the metals as the respective metal hydroxides.

Figure 12 shows a graph of the weight percent gibbsite and boehmite as a function of time upon heating gibbsite at 150 °C in with or without the presence of iron or a mixture of iron and manganese in a sealed vessel. The presence of the iron or mixture of iron and manganese did not have any measurable effect on the onset of transformation or the bulk

transformation kinetics (i.e., slope of line spanned by fraction of boehmite between 20 and 80 wt %). However, as shown in Figure 12, the addition of iron or iron and manganese did affect the quantity of bayerite in the final product. In the absence of iron or manganese, the final product cotained about 15 wt % bayerite, but only about 8 wt % when iron or iron and manganese were added. The lower bayerite content may be due in part to the lower free hydroxide concentration and higher nitrate concentration as a result of the added metal nitrate salts.

Figure 13 presents the phase concentration as a function of time at two different NaOH concentrations in a sealed contained. At 3.0 molal NaOH, the transformation of gibbsite was faster than that observed at 1.5 molal NaOH. The higher NaOH concentration also produced a higher quantity of bayerite. Tests at different NaOH concentrations in an unsealed vessel showed no significant differences in either the transformation rate or the quantity of bayerite producted.

Discussion

Based on the XRD, FTIR and TEM results, we conclude that the transformation of gibbsite to boehmite occurs by two different mechanisms depending on the water content. At low water vapor pressure gibbsite first decomposes due dehydration and becomes disordered. The dehydration of gibbsite initiates on the (001) planes. Boehmite nucleates on the internal and external surfaces of the decomposed gibbsite particles as clusters of fine crystallites. The boehmite crystallites further coalesce and grow into fibrous particles within the decomposed matrix of gibbsite.

We should point out that the direct transformation mechanism for boehmite formation is different from the dehydration mechanism reported in the calcination processes[4,10] and the thermal decomposition processes.[8,9,11-13] When we mixed gibbsite and other salts, and baked the mixed powders under dry conditions from 100°C to 150°C, no boehmite was formed over an extended period of time (7 days at 100°C and 14 hours at 150°C). Furthermore, there was little change in the crystalline structure of gibbsite as evidenced by XRD patterns.

At high water vapor pressure conditions, the transformation of gibbsite occurs by a different mechanism. In this mechanism gibbsite dissolves into solution and then crystallizes as boehmite. The TEM results suggests that the boehmite nucleation initiates either homogeneously from solution or heterogenously onto vessel walls, but not onto gibbsite particles.

The reaction kinetics for both transformation mechanisms are consistent with the Johnson-Mehl-Avrami (JMA) model (equation 1) as evidenced by the S-shaped curves in Figures 2, 6, 11 and 12. The JMA model has been widely used to express isothermal crystallization and some non-isothermal crystallization for ceramics and glasses.[14,15]

$$\alpha = 1 - \exp(-kt^n) \qquad (1)$$

where α is the time dependence of the fractional extent of crystallization, *k* and *n* are constants with respect to time *t*. The kinetic exponent *n* reveals characteristics of nucleation in the crystallization process.[16,17]

Table 2 provides the kinetic exponent *n* obtained from curve fitting the testing results. At a hydroxide concentration of 1.5 molal, gibbsite to boehmite conversions in sealed and unsealed containers gave kinetic exponents of 3.2 and 4.0, respectively. In the unsealed container, identical kinetic exponents were obtained in the presence or absence of the added salts. These results indicate a decreasing nucleation rate in the sealed container at higher vapor pressure of water and a constant nucleation rate in the unsealed container regardless of the presence or absence of added salts. The latter result suggests that there were sufficient nucleation sites to maintain a constant nucleation rate during the dehydration and decomposition of gibbsite even in the absence of precipitated iron and manganese hydroxides. This is in agreement with the fact that the gibbsite degradation preceded the formation of boehmite.

The kinetic exponents for the sealed transformations in 1.5 molal and 3 molal NaOH environment were 3.2 and 3.9 respectively, indicating the conversion at higher hydroxide concentration was much closer to a crystallization at a constant nucleation rate (i.e., kinetic exponent $n = 4$). The higher alkalinity may possibly enhance the transformation kinetics by maintaining a higher level of soluble species in solution. Since the kinetic exponent at the higher hydroxide concentration is similar to that measured for the unsealed tests, we conclude that the nucleation of boehmite was not limited by the solublized aluminum species at this condition. However, at the lower hydroxide concentration (1.5 molal NaOH), the solubility of gibbsite was reduced, which limited the rate of gibbsite dissolution and transformation to boehmite.

In the unsealed container, initiation of the gibbsite-boehmite transformation was retarded by the presence of iron or a mixture of iron and manganese (see Figure 11). Note that the addition of manganese to the iron did not significantly affect the transformation kinetics upon initiation of the bulk transformation. The addition of manganese did appear to produce a slightly longer induction time and lengthened the time for conversion of the last 20 % of gibbsite. The addition of iron or the iron/manganese mixture also did not significantly change the transformation kinetics upon initiation of bulk transformation compared to that with no added metals as evidenced by the same exponential factors (see Table 2) and similar slopes of the curves during the time period of rapid conversion (see Figure 11). We attributed the affect of the added metal salts primarily to the retardation of water evaporation. We did not quantity the rate of water loss, but the presence of additional precipitated metal hydroxides solids should retard water evaporation.

CONCLUSIONS

The transformation of gibbsite to boehmite was studied over a selected range of experimental conditions. Two pathways were unambiguously identified for hydrothermal transformation of gibbsite to boehmite: (1) dehydration of gibbsite and in situ nucleation of boehmite on and (2)gibbsite dissolution of gibbsite and nucleation of boehmite from solution. In both processes, the kinetics of conversion followed the sigmoid Johnson-Mehl-Avrami (JMA) equation. The kinetic exponent (n) from the JMA model reveals a higher nucleation rate in crystallization at higher alkalinity in a sealed container, as well as a constant nucleation rate for the direct dehydration mechanism compared with a decreasing nucleation rate from

solution mechanism at the same alkalinity. Thus we conclude that the liquid phase composition and the water vapor pressure presented to the gibbsite play critical roles in the gibbsite to boehmite transformation. Storage conditions for HLW sludges include low and high water content and elevated temperatures due to radiolytic decay. Thus, transformation of gibbsite into boehmite during storage of the HLW sludges would be expected to occur by both of the mechanisms identified in this testing. We plan to perform additional tests varying the temperature, composition and concentration of the liquid phase as well as the water content to identify conditions that inititate onset of the transformation and better quantify the roles of these variables in the gibbsite transformation.

ACKNOWLEDGEMENT

This work was supported by the Department of Energy, Office of Environmental Management, Environmental Management Science Program. XRD analyses were performed in the Environmental Molecular Sciences Laboratory, a national scientific user facility sponsored by the Department of Energy's Office of Biological and Environmental Research and located at the Pacific Northwest National Laboratory.

REFERENCES

1) Gitzen, W. H. *Alumina as A Ceramic Material, Chapter 1*. ACS: Columbus, Oh, 1970.

2) Wefers, K.; Misra, C., Oxides and Hydroxides of Aluminum, *Alcoa Technical Paper No. 19, Revised*. Aluminum Company of America.

3) Bohm V. J. Aluminum and Iron Hydroxides. *Zeitschriftfur Anorganische und A 11gemeine Chemie* **1925**, *149*, 203.

4) Day, M. K. B.; Hill, V. J. Thermal Transformations of the Aluminas and Their Hydrates. *Nature* **1952**, *170*, 539.

5) Zorpette, G. Hanford's Tank Wasteland. *Scientific Amecican*, May **1996**, 88.

6) Bunker, B. C.; Virden, J. W.; Kuhn, B.; Quinn, R. Nulcear Materials, Radioactive Tank Wastes. *Encyclopedia of Energy and the Environment*, Vol. 4. John Wiley & Sons, Inc: New York, 1995.

7) Hobbs, D. T. and Coleman, C. J. Characterization of High-Level Waste Saltcake Stored at the Savannah River Site, *Radioactive Waste Management and Env. Res*. **1999**, 21, 235.

8) Candela, L; Perlmutter, D. D. Pore Structures and Kinetics of the Thermal Decomposition of $AI(OH)_3$- *AIChE* J. **1986**, *32(9)*, 1532.

9) Candela, L.; Perlmutter, D. D. Kinetics of Boehmite Formation by Thermal Decomposition of Gibbsite. *Ind Eng. Chem. Res.* **1992**, *31*, 694.

10) Boer, J. H. de; Heuvel, A. van den; Linsen, B. G. Studies on Pore Systems in Catalysts IV. J. *Catal.* **1964**, *3*, 268.

11) Ervin, Jr., G.; Osborn, E. F. The System Al_2O_3-H_2O. *J. Geol.* **1951**, *59*, 381.

12) Krivoruchko, O.P.; Zolotovskii, B.P.; Plyasova, L.M.; Buyanov, R.A.; Zaikovskii, V.I. Boehmite Formation Mechanism in Precipitate Ageing. *React. Kinet. Catal. Lett.* **1982**, *21(1-2),* 103.

13) Sato, T. Hydrothermal Reaction of Alumina Trihydrate. *J.* Appl. *Chem.* **1960**, *10,* 414.

14) Johnson, W.A. ; Mehl, R.F. Reaction Kinetics in Processes of Nucleation and Growth. *Trans. Am. Inst. Miner. (Metall.) Eng.,* **1939**, 135, 416.

15) Avrami, M. Granulation, Phase Change, and Microstructure. *J. Chem. Phys.* **1941**, *9,* 177.

16) Christian, J.W. *The theory of Transformations in Metals and Alloys, 2nd edn.,* Pergamon: New York, 1975.

17) Malek, J. The Applicability of Johnson-Mehl-Avrami Model in the Thermal Analysis of the Crystallization Kinetics of Glasses. *Thermochimica Acta* **1995**, *267,* 61.

Table 1. Compositions of the initial solutions

Sample No.	Gibbsite, g	NaOH, g	$Fe(NO_3)_3$, g	$KMnO_4$, g	$Mn(NO_3)_2$, g	H_2O, g
1	10.0	1.2	0	0	0	20.0
2	7.0	1.2	3.0	0	0	20.0
3	7.0	1.2	1.0	1.0	1.0	20.0
4	10.0	2.4	0	0	0	20.0
5	7.0	2.4	1.0	1.0	1.0	20.0

Table 2. Kinetic exponent of Johnson-Mehl-Avrami model for the gibbsite-boehmite transformations

Transformations	n in $\alpha = 1\text{-}\exp(-kt^n)$
Sealed, 1.5 m NaOH	3.2 ± 0.16
Sealed, 3 m NaOH	3.9 ± 0.20
Unsealed, 1.5 m NaOH	4.0 ± 0.20
Unsealed, with Fe and Mn salts	4.0 ± 0.20

FIGURE CAPTIONS

Figure 1. Gibbsite to boehmite transformation in the unsealed container as monitored by XRD patterns: at 150°C for (a) 0 hr; (b) 1 hr; (c) 2 hrs; (d) 2.5 hrs; (e) 3.5 hrs; (f) 4 hrs; (g) 5.5 hrs; (h) 24 hrs.

Figure 2. The transformation process in the unsealed container as illustrated by the phase content curves.

Figure 3. FTIR spectra for the transformation in the unsealed container at 150°C for (a) 0 hr; (b) 2.5 hrs; (c) 3 hrs; (d) 3.5 hrs.

Figure 4. TEM image of a gibbsite particle after heated for 2.5 hrs in the unsealed container (a), SAD of both boehmite and gibbsite as identified on the same particle B (b); lower atomic ratio O/Al on boehmite-rich particle B than on gibbsite-rich particle A (c).

Figure 5. Bright field image with SAD of another gibbsite particle (Particle A) after heating for 2.5 hrs (a); dark field images of the gibbsite particle (b, c, d); G and B stand for gibbsite and boehmite respectively.

Figure 6. TEM image of fibrous boehmite particles generated from coagulation of boehmite flakes.

Figure 7. Gibbsite to boehmite transformation in the sealed container as monitored by XRD patterns: at 150°C for (a) 0 hr; (b) 1 hr; (c) 2 hrs; (d) 2.5 hrs; (e) 3 hrs; (f) 3.5 hrs; (g) 4 hrs; (h) 4.5 hrs; (i) 5.5 hrs; (j) 8.5 hrs; (k) 24 hrs.

Figure 8. The transformation process in the sealed container as illustrated by the phase content curves.

Figure 9. FTIR spectra for the transformation in the sealed container: at 150°C for (a) 0 hr; (b) 2 hrs; (c) 2.5 hrs; (d) 3.5 hrs; (e) 4.5 hrs; (f) 5.5 hrs; (g) 8.5 hrs; (h) 24 hrs.

Figure 10. TEM observations of the transformation at 150°C in the sealed container for (a) 0 hr, gibbsite; (b, c) 2.5 hrs, boehmite being precipitated while gibbsite being dissolved (B: boehmite, G: gibbsite); (d) 3 hrs, both boehmite and gibbsite present but not related; (e) 6.5 hrs, boehmite (Region 1) and bayerite (Region 2) generated; (f) EDS spectra of the boehmite (1) and bayerite (2).

Figure 11. Gibbsite-boehmite transformation in the presence of the salts in the unsealed container: (a) No salt; (b) Ferric nitrate only; (c) Three salts present: ferric nitrate, potassium permanganate, and manganese nitrate.

Figure 12. Gibbsite-boehmite/transformation in the presence of the salts in the sealed container.

Figure 13. Gibbsite-boehmite transformation at higher alkalinity in the sealed container: (a) Boehmite/3 M NaOH; (b) Bayerite/3 M NaOH; (c) Boehmite/1.5 M NaOH; (d) Bayerite/1.5 M NaOH.

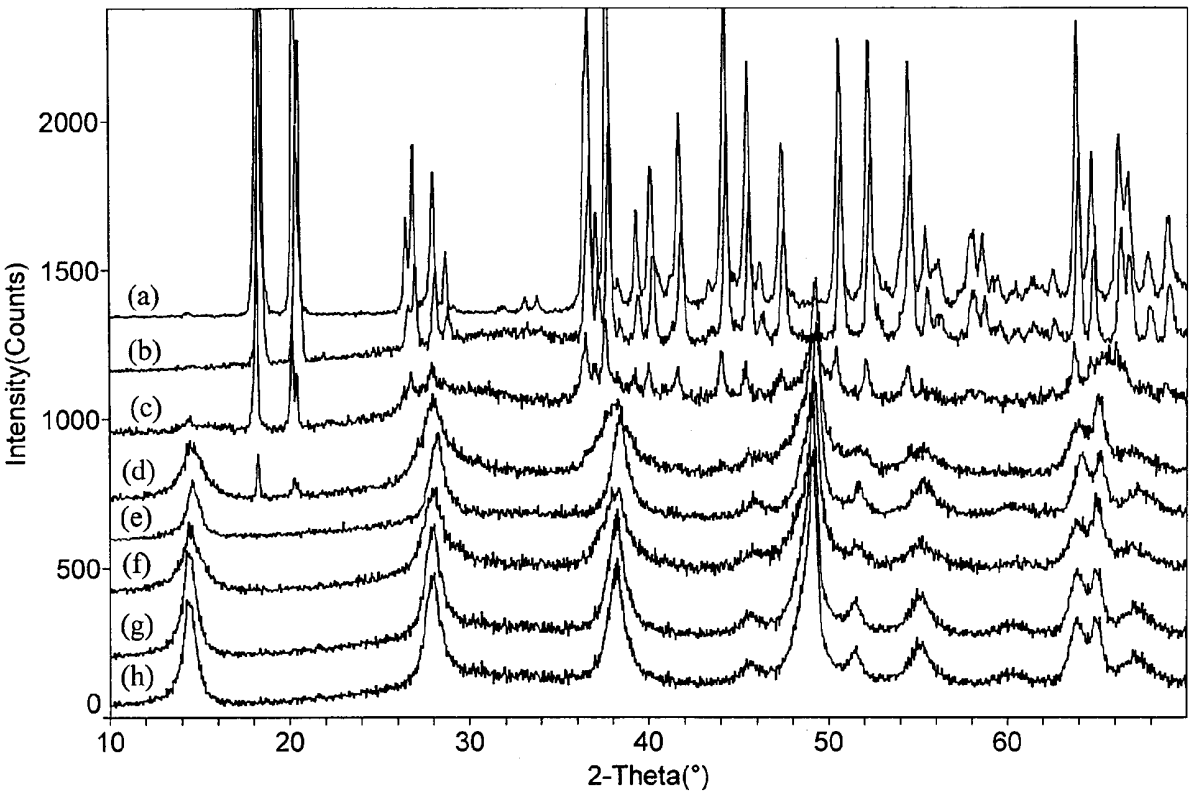

Figure 1.

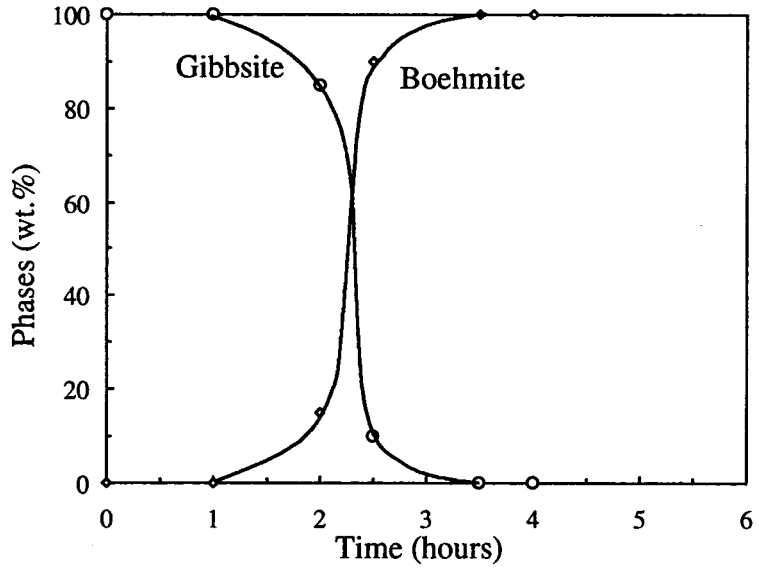

Figure 2.

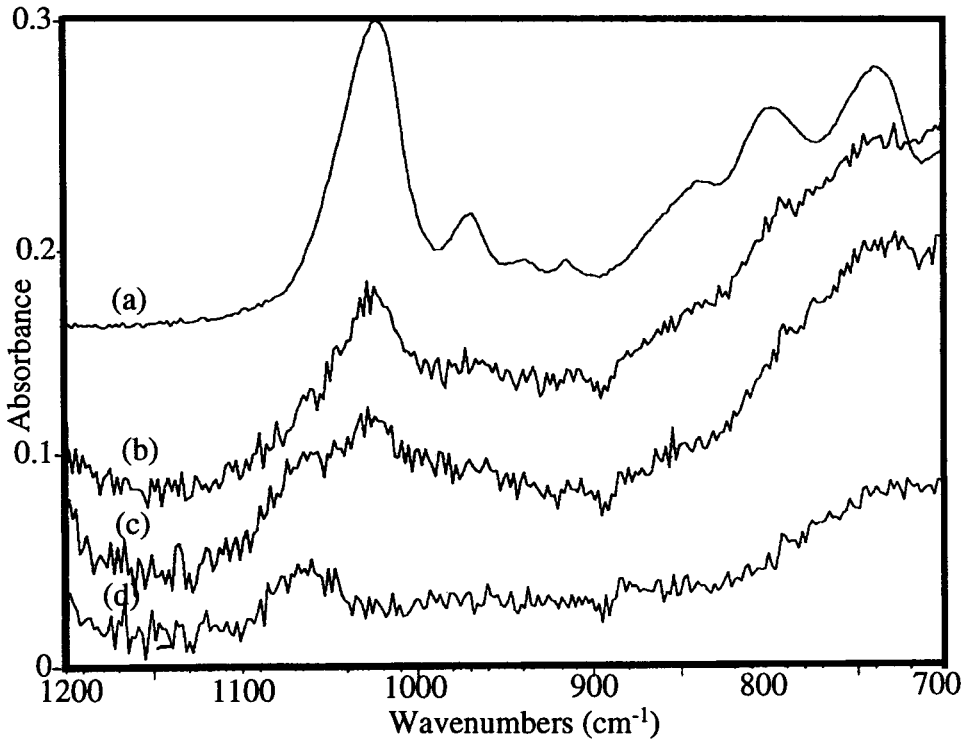
0.3
0.2
0.1
0
Absorbance
(a)
(b)
(c)
(d)
1200
1100
1000
900
800
700
Wavenumbers (cm-1)

Figure 3.

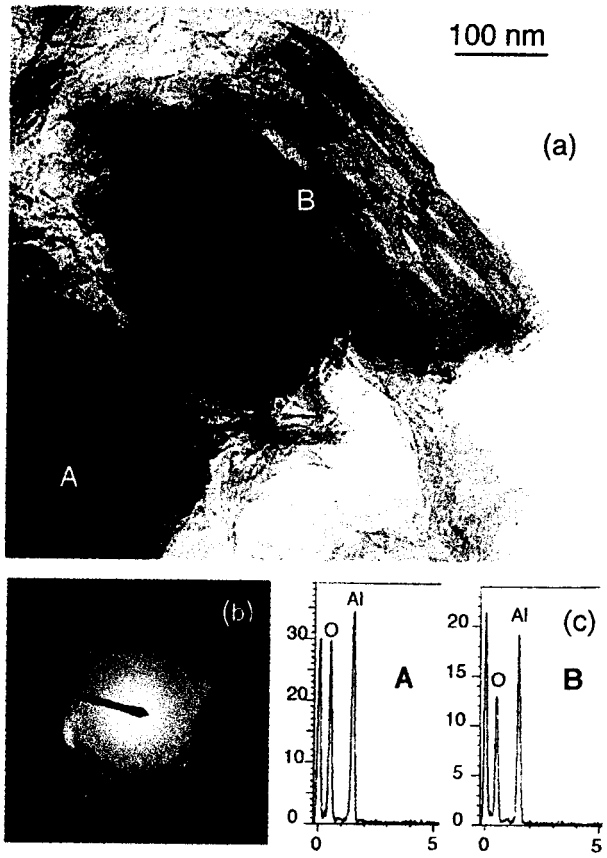

Figure 4.

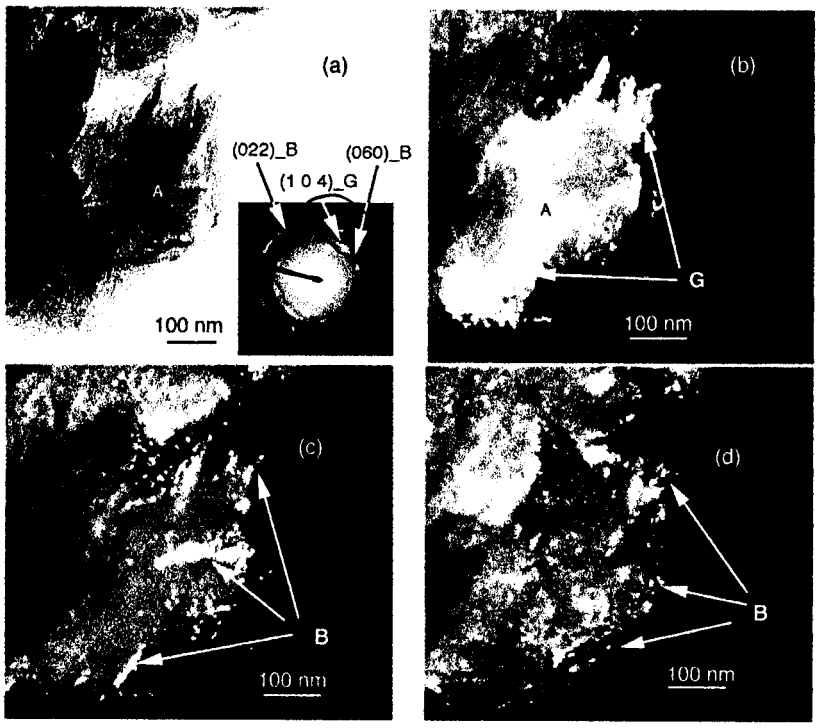

Figure 5.

Figure 6.

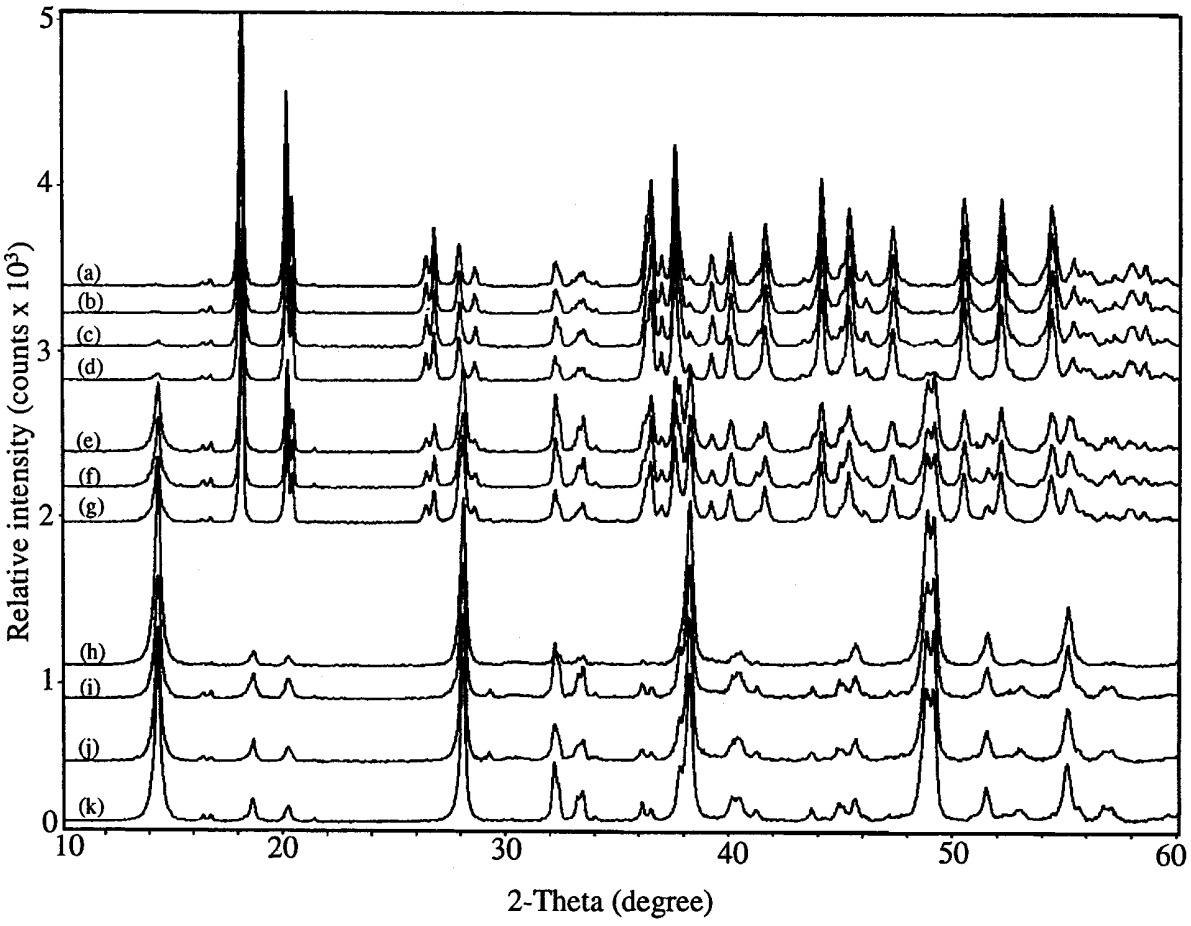
Relative intensity (counts x 10³)
2-Theta (degree)
(a)
(b)
(c)
(d)
(e)
(f)
(g)
(h)
(i)
(j)
(k)
0
1
2
3
4
5
10
20
30
40
50
60

Figure 7.

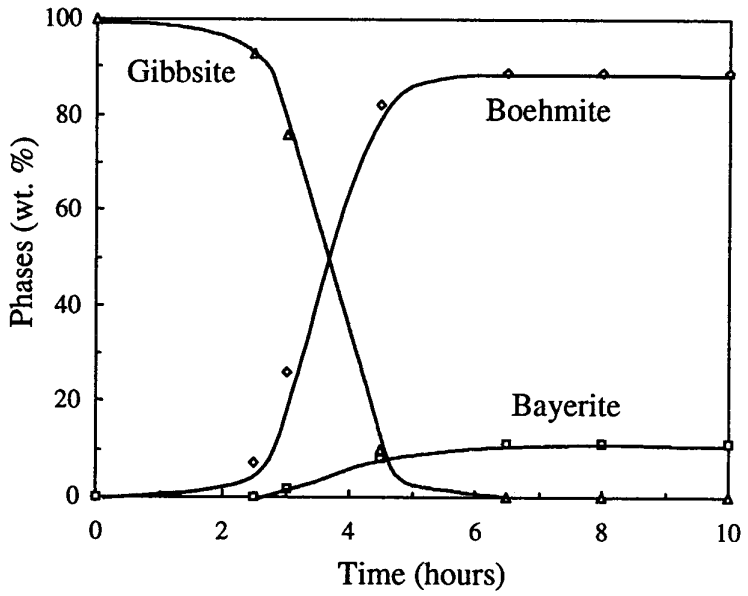

Figure 8.

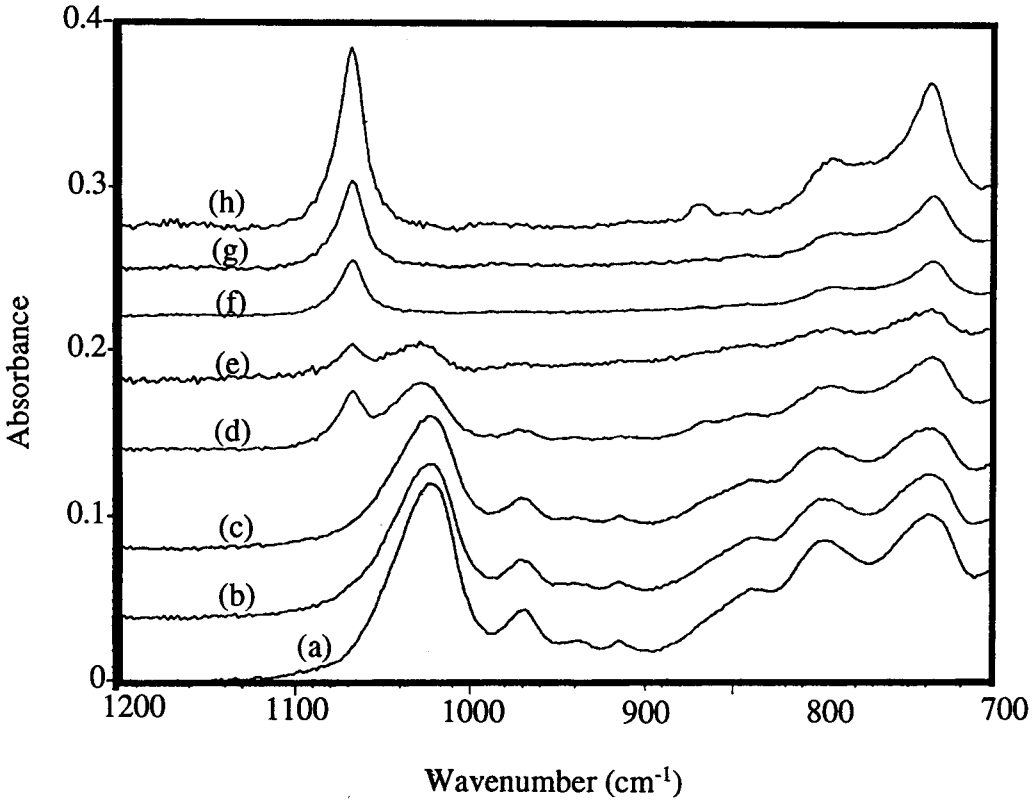

Figure 9.

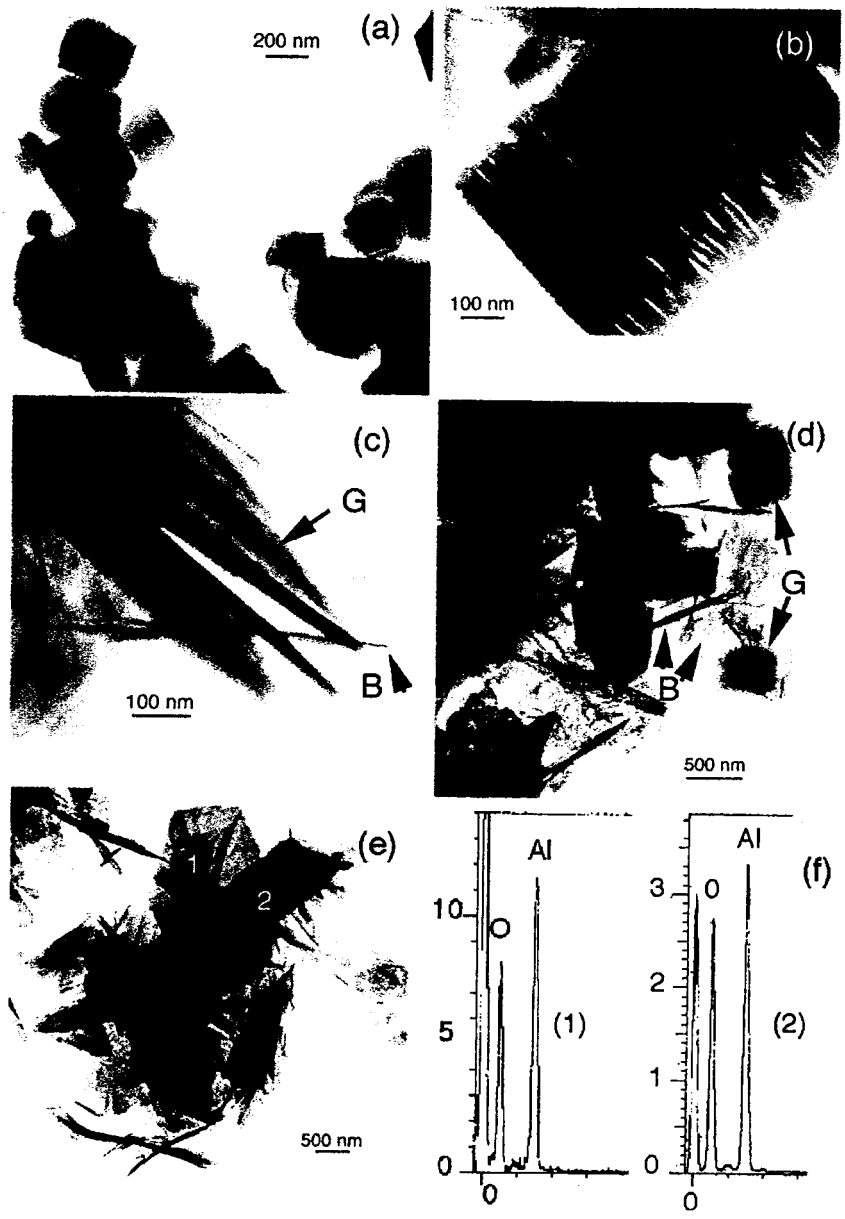
200 nm
(a)
(b)
100 nm
(c)
G
B
100 nm
(d)
G
B
500 nm
(e)
1
2
500 nm
Al
O
10
5
0
(1)
0
Al
O
3
2
1
0
(2)
0
(f)

Figure 10.

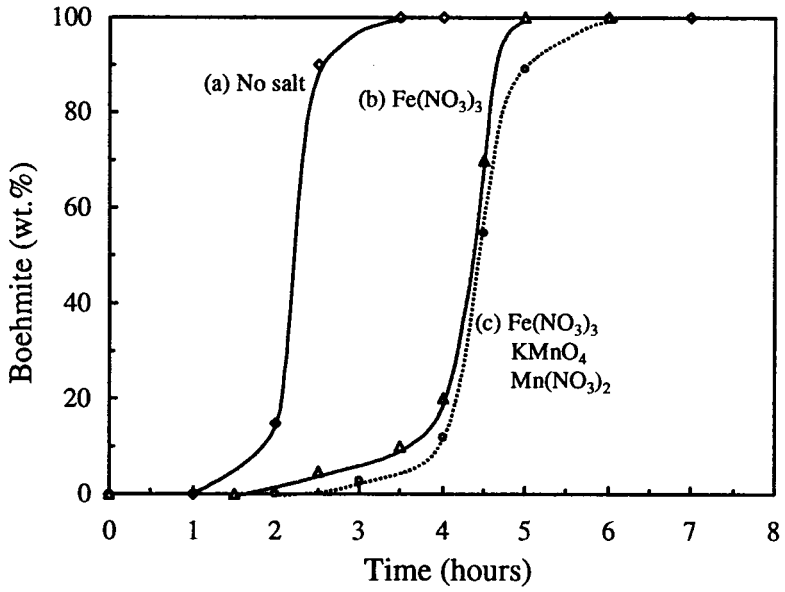

Figure 11.

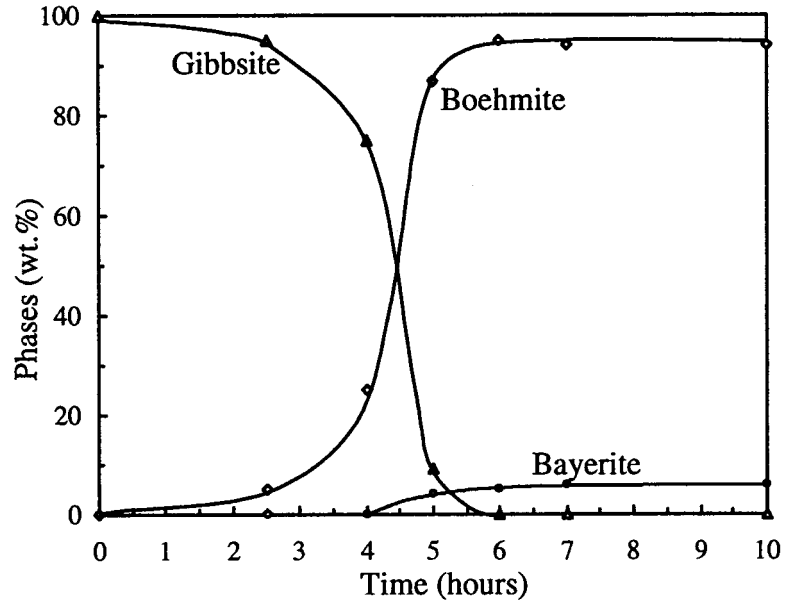

Figure 12.

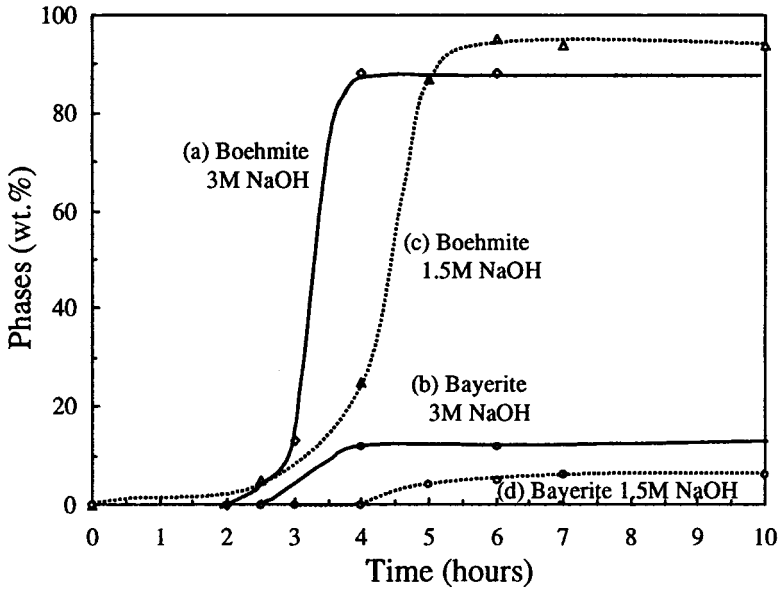
100
80
60
40
20
0
Phases (wt.%)
0
1
2
3
4
5
6
7
8
9
10
Time (hours)
(a) Boehmite
3M NaOH
(c) Boehmite
1.5M NaOH
(b) Bayerite
3M NaOH
(d) Bayerite 1.5M NaOH

Figure 13.